The curious case of cuprous chloride: Giant thermal resistance and anharmonic quasiparticle spectra driven by dispersion nesting

Saikat Mukhopadhyay,[1,*] Dipanshu Bansal,[1] Olivier Delaire,[1,2] Didier Perrodin,[3] Edith Bourret-Courchesne,[3] David J. Singh,[4] and Lucas Lindsay[1]

[1]*Materials Science and Technology Division, Oak Ridge National Laboratory, Oak Ridge, Tennessee 37831, USA*

[2]*Department of Mechanical Engineering and Materials Science and Department of Physics,*
Duke University, Durham, North Carolina 27708, USA

[3]*Materials Sciences Division, Lawrence Berkeley National Laboratory, Berkeley, California 94720, USA*

[4]*Department of Physics and Astronomy, University of Missouri, Columbia, Missouri 65211-7010, USA*

Strongly anharmonic phonon properties of CuCl are investigated with inelastic neutron-scattering measurements and first-principles simulations. An unusual quasiparticle spectral peak emerges in the phonon density of states with increasing temperature, in both simulations and measurements, emanating from exceptionally strong coupling between conventional phonon modes. Associated with this strong anharmonicity, the lattice thermal conductivity of CuCl is extremely low and exhibits anomalous, nonmonotonic pressure dependence. We show how this behavior arises from the structure of the phonon dispersions augmenting the phase space available for anharmonic three-phonon scattering processes, and contrast this mechanism with common arguments based on negative Grüneisen parameters. These results demonstrate the importance of considering intrinsic phonon-dispersion structure toward understanding scattering processes and designing new ultralow thermal conductivity materials.

Introduction. A range of traditional material design strategies have been identified to suppress thermal conductivity (κ) in thermoelectrics, thermal barrier coatings, and phase-change materials, including nanostructuring [1–3], alloying [4], doping [5], and defect engineering [6,7]. Comparatively little attention has been given to designing intrinsic properties that govern phonon propagation, such as lattice anharmonicity and phonon dispersions. Engineering thermal conductivity requires deeper theoretical understanding of these features, validated against state-of-the-art measurements. Inelastic neutron scattering (INS) can provide such microscopic insights, and recent measurements have demonstrated phonon line broadening [8–11], shifting [8,9], and mode splitting [8] due to strong anharmonic interactions. Here we present a quasiparticle signal in an unlikely anharmonic system: cubic CuCl. The anharmonicity is so pervasive that it results in an emergent spectral peak with temperature in its integrated phonon density of states (DOS), very low κ, and unusual pressure (P)-dependent κ behavior [12]. We provide fundamental insights into these features and their relationships using first-principles Boltzmann transport methods.

CuCl is a binary Ib-VII metal halide with zincblende crystal structure at ambient conditions. This is unusual, as Ia-VII alkali halides and noncuprous Ib-VII compounds tend to form rocksalt or cesium chloride structure, more typical of ionic bonding. In fact, according to Phillip's criterion for ionicity [13], CuCl is just outside the rocksalt stability range. Many properties of CuCl suggest strong anharmonicity: negative thermal expansion [14], negative Grüneisen parameters [14,15], unusual and broad Raman peaks [16–18], asymmetric phonon line shapes [19], and a rich phase diagram [20,21]. Slack and Andersson [12] measured $\kappa(P)$ of CuCl and found very low κ [<1 W/m-K at room temperature (RT)] that decreased with increasing P. This pressure response is unusual, although found in a few other systems [12,22–24], and was attributed to large negative Grüneisen parameters of transverse acoustic (TA) modes.

The present work addresses the following questions: Are there indicators of strong anharmonicity not yet seen in CuCl and other systems, and can they provide further insights into anharmonic phonon interactions? Is the unusually low κ for CuCl intrinsic (driven by phonon interactions) or extrinsic (governed by crystal quality)? Is the behavior of $\kappa(P)$ a result of negative TA Grüneisen parameters as suggested?

Experimental methodology. The Bridgman-Stockbarger technique [25] was used (gradient at melting point 8 °C/cm and crucible translation 0.75 mm/h) to melt and resolidify raw CuCl (4N purity, Sigma-Aldrich) in a sealed quartz ampoule. Material was white in color and powder x-ray diffraction confirmed zincblende structure.

Phonon DOS was measured using the time-of-flight wide angular-range chopper spectrometer at the Spallation Neutron Source at Oak Ridge National Laboratory [26]. The sample was encased in a thin-walled aluminum can using a closed-cycle helium refrigerator for $5\,\text{K} < T < 300\,\text{K}$ and a low-background resistive furnace for $300\,\text{K} < T < 580\,\text{K}$. For low T, the sample chamber was filled with low-pressure helium to facilitate cooling. An oscillating radial collimator was used to minimize background scattering from sample environment. Two incident neutron energies $E_i = 25$ and 55 meV were used to measure low-energy modes and the full spectrum, respectively. Energy resolution (full width at half maximum) at the elastic line was $\sim$1.2 and 2.2 meV, respectively. The measured signal was transformed to momentum $|\mathbf{Q}|$ and energy transfer E using the MANTID software [27] and two-dimensional intensity maps for dynamical susceptibility $\chi''(|\vec{Q}|,E) = [1 - e^{-(E/k_B T)}]S(|\vec{Q}|,E)$ were obtained from

*Corresponding author: mukhopadhyas@ornl.gov

the dynamical structure factor $S(|\vec{Q}|, E)$. The DOS was obtained by integrating from $3 < |\vec{Q}| < 7\,\text{Å}^{-1}$ for $E_i = 55$ meV and $2 < |\vec{Q}| < 5\,\text{Å}^{-1}$ for $E_i = 25$ meV, accounting for background, multiphonon scattering, and the elastic peak [28]. The DOS $g(E) = \sum_k w_k g_k(E)/\sum_k w_k$ is constructed from contributions of each element labeled by k and weighted by $w_k = \sigma_k/m_k$ with σ_k being neutron-scattering cross section and m_k mass: $w_{Cu} = 0.1264$ and $w_{Cl} = 0.4739$ barns/amu.

Theoretical methodology. Mode contributions to DOS; $g_{\vec{q}j}(E) = \sum_k |\vec{\varepsilon}_{k\vec{q}j}|^2 \delta[E - \omega_{\vec{q}j}^{\text{anh}}(E)]$, also known as spectral function, were determined from first principles where $\vec{\varepsilon}_{k\vec{q}j}$ is the eigenvector of the kth atom with wave vector $\vec{q}$ in branch j, and $\omega_{\vec{q}j}^{\text{anh}}(E)$ is the anharmonic frequency corrected via phonon interactions: $\omega_{\vec{q}j}^{\text{anh}}(E) = \sqrt{\omega_{\vec{q}j}^2 + 2\omega_{\vec{q}j}[\Delta_3(E) + \Delta_4 + \Delta_{\text{exp}}]}$, where Δ_{exp}, $\Delta_3(E)$, and Δ_4 are line shifts due to lattice expansion [29], third- and fourth-order anharmonicity [30], respectively, and $\omega_{\vec{q}j}$ is the harmonic frequency. These shifts depend on T and are built from interatomic force constants (IFCs) described below. The delta function in $\omega_{\vec{q}j}$ is represented by a Lorentzian:

$$\delta[E - \omega_{\vec{q}j}^{\text{anh}}(E)] = \frac{\sigma_{\vec{q}j}(E)}{\pi\{\sigma_{\vec{q}j}^2(E) + [E - \omega_{\vec{q}j}^{\text{anh}}(E)^2]\}}, \quad (1)$$

where $\sigma_{\vec{q}j}(E)$ is the linewidth [30]:

$$\sigma_{\vec{q}j}(E) = \frac{18}{\hbar^2} \sum_{\vec{q}'j',\vec{q}''j''} |V_3(\vec{q}j,\vec{q}'j',\vec{q}''j'')|^2 \Delta(\vec{q} + \vec{q}' + \vec{q}'')[(n_{\vec{q}'j'} + n_{\vec{q}''j''} + 1)\{\delta(\omega_{\vec{q}'j'} + \omega_{\vec{q}''j''} - E) - \delta(\omega_{\vec{q}'j'} + \omega_{\vec{q}''j''} + E)\},$$

$$+ (n_{\vec{q}''j''} - n_{\vec{q}'j'})\{\delta(\omega_{\vec{q}'j'} - \omega_{\vec{q}''j''} - E) - \delta(\omega_{\vec{q}'j'} - \omega_{\vec{q}''j''} + E)\}] \quad (2)$$

where V_3 are three-phonon scattering matrix elements [30], $n_{\vec{q}j}$ are Bose factors, and Δ ensures crystal momentum conservation. Replacing E with $\omega_{\vec{q}j}$, Eq. (2) becomes the inverse of the lifetimes $(1/\tau_{\vec{q}j})$ which enter the expression for the thermal conductivity: $\kappa = \sum_{\vec{q}j} C_{\vec{q}j} v_{\vec{q}j}^2 \tau_{\vec{q}j}$, with $C_{\vec{q}j}$ being mode-specific heat and $\vec{v}_{\vec{q}j}$ being phonon velocity.

Harmonic and anharmonic IFCs were calculated using finite displacements in VASP-PHONOPY [31] and VASP-PHONO3PY [32], respectively, and the projector augmented wave method [33,34] following the Perdew, Burke, and Ernzerhof (PBE) approach [35,36]. The optimized $P = 0$ lattice parameter [5.426 Å] compares favorably with its measured counterpart [5.402 Å] [37] with typical overestimation from PBE [38]. Third-order IFCs were truncated at fifth-nearest-neighbor interactions, while fourth-order IFCs for determining Δ_4 were truncated at second-nearest neighbors [39]. The phonon Boltzmann transport equation (PBTE) within the relaxation time approximation was employed to determine phonon lifetimes and κ [32]. We find $\kappa = 1.41$ W/m-K at RT similar to that found previously for CuCl, $\kappa = 1.44$ W/m-K [32]. We further verified our methods with independent IFC and κ calculations using the QUANTUM ESPRESSO package [40] and a full iterative solution of the PBTE [24]. These gave similar results to those presented here, verifying the robustness of these methods.

Results. Figure 1 gives calculated phonon dispersions of CuCl at $P = 0, 0.74$ and 4.5 GPa with measured INS data at $P = 0$ and $T = 4$ K from previous work [41]. The calculated acoustic spectrum compares well with measured values, while optic frequencies are underestimated due to the PBE approach [38]. Despite this, calculated specific heat [39] and bulk modulus (48.6 GPa) compare reasonably with measured data (54.5 GPa [42]). Despite having relatively light masses, the overall CuCl frequency scale is low, comparable to systems with much heavier masses, e.g., InSb [43]. Thus CuCl acoustic phonons have small group velocities and carry less heat than in typical zincblende materials.

Interestingly, the optic branches dip in frequency on approaching the Γ point, a behavior not seen in other zincblende systems and similar to that in SnTe and PbTe [8], which are near-ferroelectric phase transitions unlike CuCl. In PbTe this gave unusual transverse optic (TO) spectra due to dispersion nesting: *a large number of phonon interactions with the same frequency difference of two modes.* In CuCl there is also nesting behavior: ~ 2 THz frequency differences for TO and longitudinal acoustic (LA) modes for much of the Brillouin zone. In addition there is further ~ 2 THz nesting behavior between LA and TA modes (see Fig. 1). The optic dispersion dip also gives a smaller frequency gap between acoustic and optic branches and larger optic bandwidth, both features shown to reduce κ via strong acoustic-optic coupling [44,45].
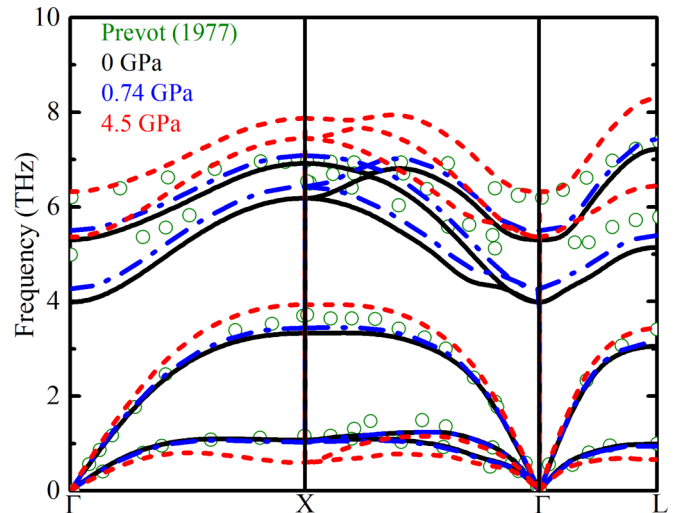

FIG. 1. Phonon dispersions of CuCl at $P = 0$ (black), $P = 0.74$ GPa (blue), and $P = 4.5$ GPa (red). Green circles give measured data for $P = 0$ [41].
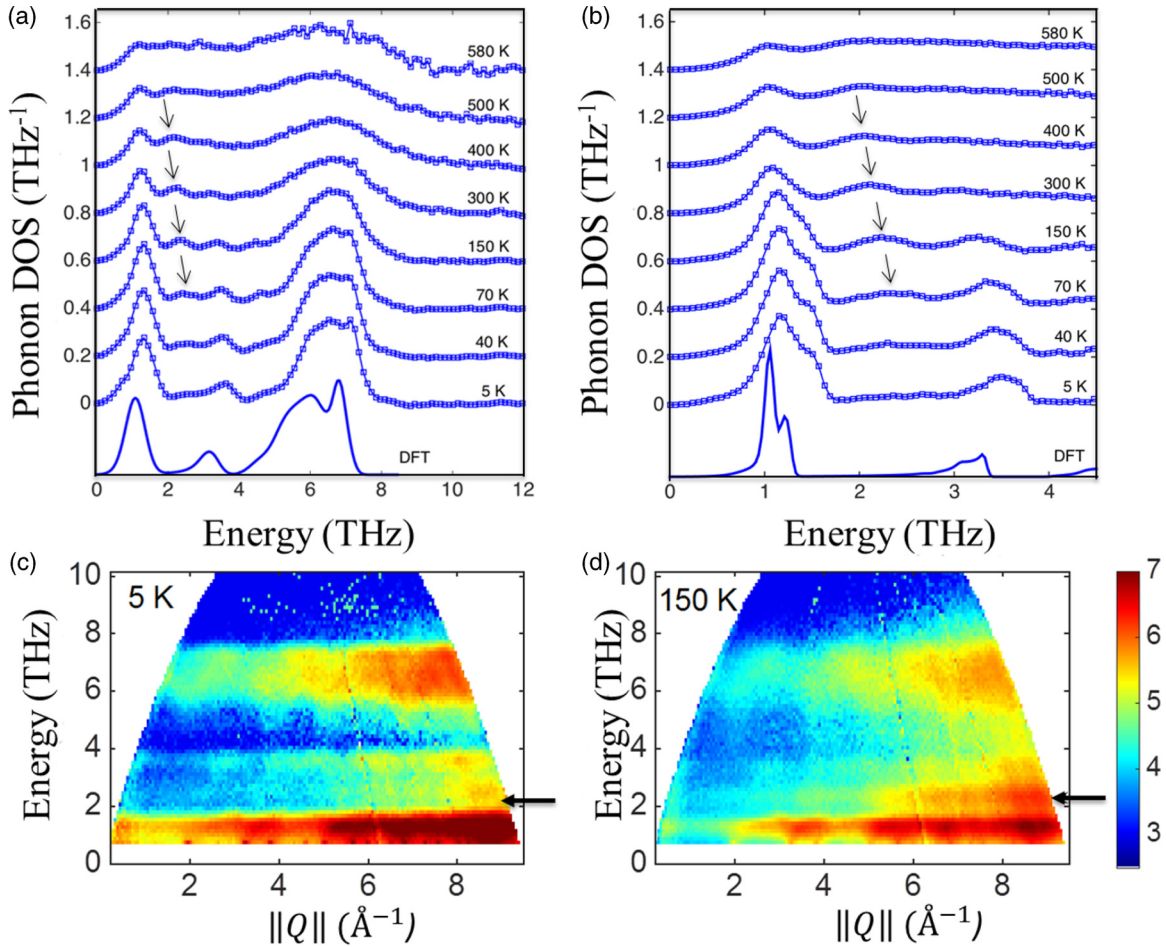
FIG. 2. Phonon DOS of CuCl from INS for various T with incident neutron energy (E_i): (a) 55 meV and (b) 25 meV. The solid blue curves give the calculated neutron-weighted DOS at experimental resolution. Dynamical susceptibility (log scale) measured at (c) 5 K and (d)150 K for $E_i = 25$ meV. The presence (absence) of emerging quasiparticle peak at $T > 150$ K ($T = 5$ K) is marked with arrows in each figure.

The origin of the low-frequency dispersion and soft Γ-point optic modes in CuCl likely arises from the large ionic radius mismatch of Cl and Cu atoms, 1.67 and 0.74 Å, respectively [46] (Shannon crystal radius; we quote the value for VI coordinated Cl$^-$ since IV coordinated is not available). The lighter Cl ions have high weight in the optic modes. However, due to their size they interact both with the Cu and significantly with each other. At Γ, the optic modes consist of Cl$^-$ and Cu ions moving against each other, while maintaining the Cl-Cl distance. Away from Γ the mode modulates Cl-Cl distances, which is unfavorable. For example, at the X-point TO modes have large Cl atoms more strongly interacting with each other, giving effectively stiffer forces. This underlies the optic dip and observed nesting behavior.

The anharmonicity, acoustic-optic coupling, and nesting behavior in CuCl is so prevalent that it manifests itself in the integrated phonon DOS and κ. Figures 2(a) and 2(b) show the measured DOS of CuCl versus neutron energy transfer from INS for varying T. First-principles calculations at $P = 0$ compare favorably with low-T measured spectra, though peaks are softer by $\sim$0.2 THz. Strikingly, for T increasing from 5 to 150 K, an additional quasiparticle peak emerges at $\sim$2.3 THz (arrows in Fig. 2) in a frequency region where none are expected. This emerging peak gains weight

from surrounding features as heating causes broadening and decreasing intensity for peaks at $\sim$1.2 THz (TA modes) and 3.5 THz (LA modes). Overall broadening is expected given the large thermal displacement parameter of Cu ions [47]. The dynamical susceptibility of CuCl at 5 and 150 K in Figs. 2(c) and 2(d) gives further evidence of this emergent peak for $T = 150$ K, absent at $T = 5$ K. This feature was not found in previous neutron studies [19,41], though other anharmonic features were observed: unusual TO line shapes [41] and immeasurable LA modes for $T > 200$ K [19].

To understand the origin of this unusual emergent DOS peak, we calculated mode contributions to DOS, $g_{\vec{q}j}(E)$, including anharmonic line shifts and broadenings for $T = 5$ K. This differs from the standard harmonic calculation shown in Fig. 2(a), which shows no evidence of a peak $\sim$2 THz. In contrast, even at $T = 5$ K, calculations including anharmonicity exhibit a broad peak just above 2 THz in the total DOS, similar to that observed in the measured data at higher T. Exploring this further, Fig. 3(a) shows the partition of mode contributions $g_{\vec{q}j}(E)$ for $E = 1.088$ THz (sharp TA peak, typical resonance behavior) and for $E = 2.055$ THz (broad emergent peak, anomalous behavior).

At resonance, $E \approx \omega_{\vec{q}j}^{\mathrm{anh}}(E)$ in Eq. (1), the DOS contribution from mode $\vec{q}j$ can become large, with magnitudes dictated by
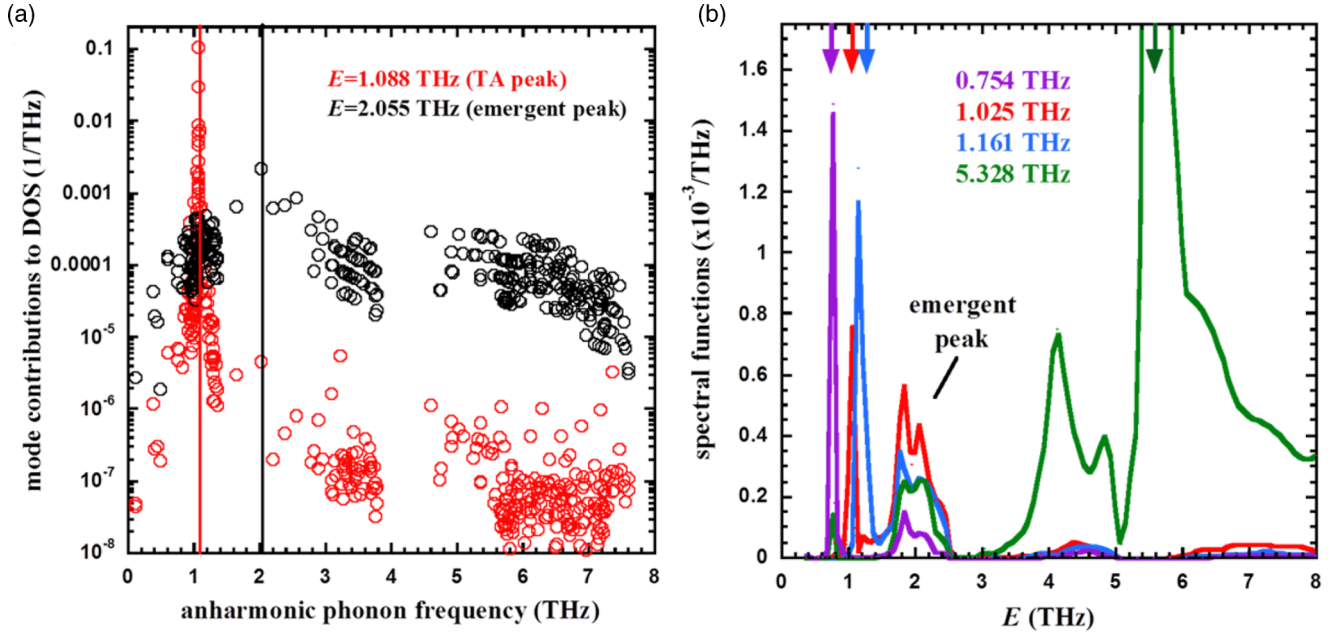
FIG. 3. (a) Calculated mode contributions to DOS vs $\omega_{\vec{q}j}^{\mathrm{anh}}$ for energy transfer $E = 1.088$ THz (red circles, TA peak) and $E = 2.055$ THz (black circles, emergent peak) at $T = 5$ K. Vertical lines depict E for each case. Red circles demonstrate typical resonant behavior at the TA peak, while black circles give anomalous contributions far from resonance to the emergent peak. (b) Calculated spectral functions (line shapes) for randomly selected phonons with various polarizations and frequencies. Colored arrows designate location of typical peak behavior, $E \approx \omega_{\vec{q}j}^{\mathrm{anh}}(E)$.

the linewidth $\sim 1/\sigma_{\vec{q}j}(E)$. Thus, weakly damped modes have a sharp, symmetric Lorentzian shape. Flat dispersion surfaces, for which many such modes contribute at a given E, generally give peaks in the DOS (van Hove singularities [48]). For the TA peak in Fig. 3(a) only modes with frequencies near 1 THz contribute appreciably. In contrast, for the emergent peak ~ 2 THz DOS mode contributions over a wide range of frequencies and polarizations are significant. For large linewidths, even "off-resonance" ($E \neq \omega_{\vec{q}j}^{\mathrm{anh}}$) mode contributions scale as $\sim 1/\sigma_{\vec{q}j}(E)$, although they are smaller as demonstrated by the "off-resonance" DOS contributions for $E = 2.055$ THz compared to those at resonance for $E = 1.088$ THz. However, numerous modes meet this condition, and contributions over the entire spectrum accumulate to give rise to the emergent peak in the CuCl DOS.

Figure 3(b) shows spectral functions (i.e., line shapes) for randomly selected modes. The line shapes strongly deviate from typical symmetric Lorentzian behavior of weakly damped vibrations. Maradudin and Fein [49] pointed out that large linewidths or -shifts (strong anharmonicity) can cause such deviations. As seen in Fig. 3(b), the sampled modes have satellite features at ~ 2 THz, which contribute to building the emergent quasiparticle spectra. We calculated the spectral functions including only anharmonic line shifts with a constant broadening factor for all modes. For this case, the emergent peak disappears, elucidating that the broadening [Eq. (2)] is responsible for this behavior. Again, for these ~ 2 THz off-resonance peaks $g_{\vec{q}j}(E) \sim 1/\sigma_{\vec{q}j}(E)$, and since V_3 is independent of E in Eq. (2), the emergent peak is governed by the energy-conserving delta functions, which peak for $E = 2$ THz due to matching phonon-frequency differences: dispersion nesting.

To further verify that dispersion nesting is the governing feature of these unusual line shapes and emergent DOS peak, we calculate Eq. (2) without V_3 and the prefactor $[\sigma_{\vec{q}j}(E) \rightarrow N_{\vec{q}}(E)]$, which then simply measures the number of interactions allowed at each E by conservation of energy and momentum, or measures the dispersion nesting behavior. We label this expression $N_{\vec{q}}(E)$ and note that it is independent of branch index and is weighted by Bose factors, thus is T-dependent. Similar expressions are referred to in the literature as joint- or two-phonon density of states [31,41,50]. The black curve in Fig. 4 gives $N_{\vec{q}}(E)$ versus E for $T = 5$ K and $P = 0$.

A large spike in $N_{\vec{q}}(E)$ occurs at ~ 2 THz, demonstrating strong nesting behavior exactly at the frequency of the emergent peak in the measured DOS. This $N_{\vec{q}}(E)$ peak position is independent of T and demonstrates that a large number of scatterings are available to modes near this frequency, comprising both coalescence (LA/TO) and decay (LA/TA) processes.

These anharmonic scattering features also play a critical role in determining phonon transport, for which CuCl demonstrates atypical behavior. Calculated $\kappa(P)$ of CuCl at RT is shown in Fig. 5 with measured data [12]. Our first observation from Fig. 5 is ultralow κ values for both calculated (1.42 W/m-K at $P = 0$) and measured data [12] (0.75 W/m-K at $P \sim 0.5$ GPa). The low κ is surprising as typical values for zincblende systems are much higher (ranging from diamond $\kappa \sim 2300$ W/m-K [52] to InSb $\kappa \sim 19$ W/m-K [53] at RT). However, the low κ is not surprising when compared to other alkali chlorides with rocksalt structure, e.g., NaCl, KCl and RbCl with RT κ values 5.84 W/m-K [54], 6.40 W/m-K [55], and 2.33 W/m-K [23], respectively, still larger than that of CuCl. Even the prominent thermoelectric material PbTe has
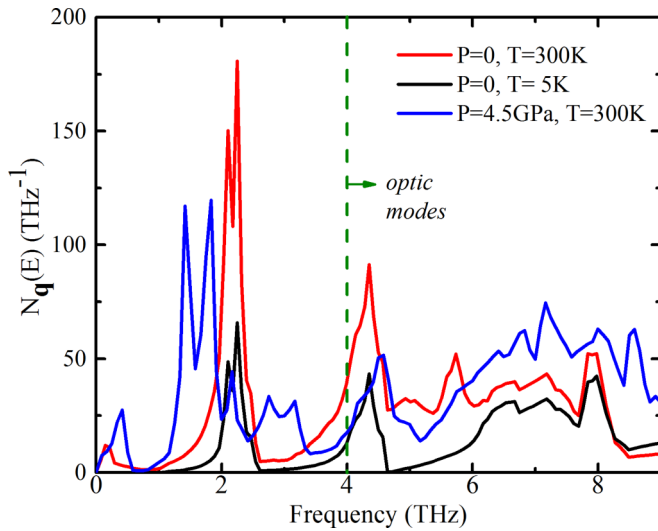
FIG. 4. $N_{\vec{q}}(E)$ vs frequency for $T = 5\,\text{K}, P = 0$ (black curve), $T = 300\,\text{K}, P = 0$ (red curve), and $T = 300\,\text{K}, P = 4.5\,\text{GPa}$ (blue curve). Bose factors reduce $N_{\vec{q}}(E)$ for $T = 5\,\text{K}$, thus the black curve is multiplied by five for better visibility. These curves correspond to $\vec{q} = (0.17, 0, 0.17)$ in units of $2\pi/a$, where a is the lattice constant. Other randomly sampled q points give nearly identical behavior.

larger $\kappa \sim 2.37\,\text{W/m-K}$ [56] at RT. The discrepancy between calculated and measured κ values may be caused by extrinsic effects (e.g., grain boundaries). Measurements were obtained from compressed powder samples [12] with little reported on crystal quality. To gain further insights, we calculated $\kappa(P)$ including boundary scattering [57] with size adjusted to fit
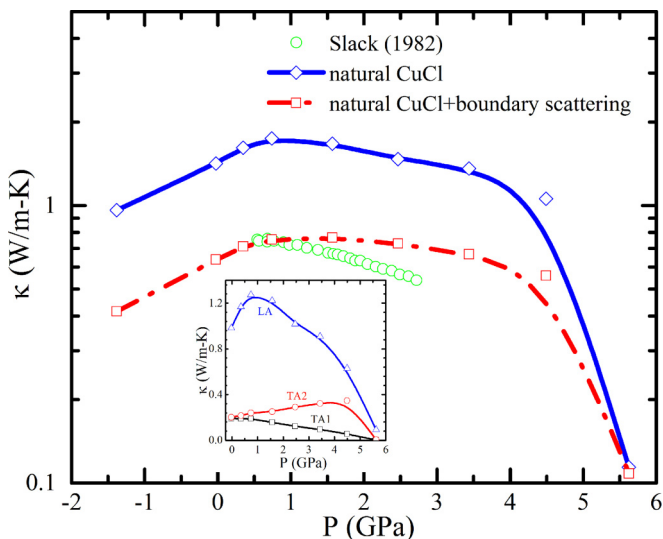

FIG. 5. Calculated κ vs P without boundary scattering (solid blue curve) and with a 60-nm boundary length (dashed red curve). κ values are also shown for isotropic tensile strain ($P < 0$). The giant reduction in κ for $P = 5.6\,\text{GPa}$ (zincblende phase) is indicative of significant TA softening and a known pressure-induced phase transition [51]. Green circles give measured data [12]. Contributions to κ for TA1 (black squares), TA2 (red circles), and LA (blue triangles) branches are shown in the inset.

the low-P measured κ. This gives an empirical grain size of $0.06\,\mu\text{m}$, much smaller than the reported average grain size of $10\,\mu\text{m}$, which gives little additional thermal resistance.

For $P > 0.74\,\text{GPa}$, both calculated and measured $\kappa(P)$ decrease with increasing P, an unusual behavior as κ typically increases [57,58] due to increasing acoustic velocities and reduced acoustic-optic coupling as optic frequencies shift higher. Previously, decreasing $\kappa(P)$ was attributed to increasingly negative TA Grüneisen parameters [12], however, TA contributions to the calculated κ are minimal (inset to Fig. 5). Instead, LA modes dominate κ for all P, thus the $\kappa(P)$ behavior is not directly caused by this, although TA softening does affect LA mode lifetimes as discussed below. Another unusual feature in Fig. 5 is the nonmonotonic behavior of the calculated $\kappa(P)$, which suggests an interplay of physical properties competing to govern thermal transport.

For $P < 0.74\,\text{GPa}$, LA modes have relatively constant lifetimes with increasing P, while their group velocities increase, thus giving increasing $\kappa(P)$. Constant LA lifetimes are a consequence of unchanged Grüneisen parameters (Supplemental Material, Fig. S2 [39]) and $N_{\vec{q}}(E)$ as the TA branch is unaffected. For $P > 0.74\,\text{GPa}$, LA velocities continue to increase, however, the TA branch softens. TA softening and LA hardening drive the branches apart, which gives increased scattering for a broader range of LA phonons [24]. As seen in Fig. 4, for $P = 4.5\,\text{GPa}$ the $\sim 2\,\text{THz}$ $N_{\vec{q}}(E)$ peak is smaller and shifted to lower frequency; however, a broader frequency range has larger $N_{\vec{q}}(E)$ values (area under the curves for acoustic modes: 74.3 for $P = 0$ and 101.5 for $P = 4.5\,\text{GPa}$) than that at lower P. The resulting reduced phonon lifetime (Supplemental Material, Fig. S3 [39]) more than compensates increasing LA velocities to give decreasing κ with increasing P for $P > 0.74\,\text{GPa}$. The unusual $\kappa(P)$ behavior of CuCl is not a result of increasing anharmonicity of TA modes, but rather a consequence of changing dispersion structure as TA modes soften and LA modes harden.

Summary. Neutron-scattering measurements of phonon DOS of CuCl reveal an unusual temperature-dependent quasiparticle peak at $\sim 2\,\text{THz}$. First-principles calculations demonstrate that this emergent peak is a result of a large number of anharmonically coupled phonon interactions for this frequency range: dispersion nesting. Strong anharmonicity also gives rise to ultralow thermal conductivity (κ) and its unusual pressure-dependent behavior: increasing κ with increasing pressure (P) for small P then decreasing with further compression. This behavior arises from competing factors: increasing group velocities and increased scattering of LA modes, not from anharmonicity of TA phonons as previously hypothesized. This work demonstrates the successful collaboration of theory and experiment toward identifying and understanding a novel quasiparticle DOS feature important for understanding unique anharmonic properties of solids, especially pertaining to thermal transport for applications such as thermoelectricity.

[1] X. W. Wang, H. Lee, Y. C. Lan, G. H. Zhu, G. Joshi, D. Z. Wang, J. Yang, A. J. Muto, M. Y. Tang, J. Klatsky, S. Song, M. S. Dresselhaus, G. Chen, and Z. F. Ren, Appl. Phys. Lett. **93**, 193121 (2008).

[2] M. S. Toprak, C. Stiewe, D. Platzek, S. Williams, L. Bertini, E. C. Muller, C. Gatti, Y. Zhang, M. Rowe, and M. Muhammed, Adv. Funct. Mater. **14**, 1189 (2004).

[3] J. R. Sootsman, R. J. Pcionek, H. J. Kong, C. Uher, and M. G. Kanatzidis, Chem. Mater. **18**, 4993 (2006).

[4] C. Bera, N. Mingo, and S. Volz, Phys. Rev. Lett. **104**, 115502 (2010).

[5] C. M. Bhandari and D. M. Rowe, J. Phys. D.: Appl. Phys. **16**, L75 (1983).

[6] G. H. Zhu, H. Lee, Y. C. Lan, X. W. Wang, G. Joshi, D. Z. Wang, J. Yang, D. Vashaee, H. Guilbert, A. Pillitteri, M. S. Dresselhaus, G. Chen, and Z. F. Ren, Phys. Rev. Lett. **102**, 196803 (2009).

[7] D. M. Rowe and V. S. Shukla, J. Appl. Phys. **52**, 7421 (1981).

[8] C. W. Li, O. Hellman, J. Ma, A. F. May, H. B. Cao, X. Chen, A. D. Christianson, G. Ehlers, D. J. Singh, B. C. Sales, and O. Delaire, Phys. Rev. Lett. **112**, 175501 (2014).

[9] T. Lan, C. W. Li, J. L. Niedziela, H. Smith, D. L. Abernathy, G. R. Rossman, and B. Fultz, Phys. Rev. B **89**, 054306 (2014).

[10] J. Suda and T. Sato, J. Phys. Soc. Jpn. **66**, 1707 (1997).

[11] X. L. Tang and J. J. Dong, Proc. Natl. Acad. Sci. USA **107**, 4539 (2010).

[12] G. A. Slack and P. Andersson, Phys. Rev. B **26**, 1873 (1982).

[13] J. C. Phillips, Rev. Mod. Phys. **42**, 317 (1970).

[14] T. H. K. Barron, J. A. Birch, and G. K. White, J. Phys. C: Solid State Phys. **10**, 1617 (1977).

[15] R. C. Hanson, K. Helliwel, and C. Schwab, Phys. Rev. B **9**, 2649 (1974).

[16] I. P. Kaminow and E. H. Turner, Phys. Rev. B **5**, 1564 (1972).

[17] M. Krauzman, R. M. Pick, H. Poulet, G. Hamel, and B. Prevot, Phys. Rev. Lett. **33**, 528 (1974).

[18] J. E. Potts, R. C. Hanson, C. T. Walker, and C. Schwab, Phys. Rev. B **9**, 2711 (1974).

[19] B. Hennion, B. Prevot, M. Krauzman, R. M. Pick, and B. Dorner, J. Phys. C: Solid State Phys. **12**, 1609 (1979).

[20] C. W. Chu, A. P. Rusakov, S. Huang, S. Early, T. H. Geballe, and C. Y. Huang, Phys. Rev. B **18**, 2116 (1978).

[21] S. Hull and D. A. Keen, Phys. Rev. B **50**, 5868 (1994).

[22] O. Andersson and A. Inaba, Phys. Chem. Chem. Phys. **7**, 1441 (2005).

[23] P. Andersson, J. Phys. C: Solid State Phys. **18**, 3943 (1985).

[24] L. Lindsay, D. A. Broido, J. Carrete, N. Mingo, and T. L. Reinecke, Phys. Rev. B **91**, 121202 (2015).

[25] B. Perner, J. Cryst. Growth **6**, 86 (1969).

[26] M. B. Stone, J. L. Niedziela, D. L. Abernathy, L. DeBeer-Schmitt, G. Ehlers, O. Garlea, G. E. Granroth, M. Graves-Brook, A. I. Kolesnikov, A. Podlesnyak, and B. Winn, Rev. Sci. Instrum. **85**, 045113 (2014).

[27] O. Arnold, J. C. Bilheux, J. M. Borreguero, A. Buts, S. I. Campbell, L. Chapon, M. Doucet, N. Draper, R. F. Leal, M. A. Gigg, V. E. Lynch, A. Markvardsen, D. J. Mikkelson, R. L. Mikkelson, R. Miller, K. Palmen, P. Parker, G. Passos, T. G. Perring, P. F. Peterson, S. Ren, M. A. Reuter, A. T. Savici, J. W. Taylor, R. J. Taylor, R. Tolchenov, W. Zhou, and J. Zikoysky, Nucl. Instrum. Methods Phys. Res., Sect. A **764**, 156 (2014).

[28] D. Bansal, C. W. Li, A. H. Said, D. L. Abernathy, J. Q. Yan, and O. Delaire, Phys. Rev. B **92**, 214301 (2015).

[29] S. Narasimhan and D. Vanderbilt, Phys. Rev. B **43**, 4541 (1991).

[30] R. A. Cowley, Rep. Prog. Phys. **31**, 123 (1968).

[31] A. Togo, F. Oba, and I. Tanaka, Phys. Rev. B **78**, 134106 (2008).

[32] A. Togo, L. Chaput, and I. Tanaka, Phys. Rev. B **91**, 094306 (2015).

[33] P. E. Blochl, Abstr. Pap. Am. Chem. Soc. **209**, 115-PHYS (1995).

[34] G. Kresse and D. Joubert, Phys. Rev. B **59**, 1758 (1999).

[35] J. P. Perdew, K. Burke, and M. Ernzerhof, Phys. Rev. Lett. **77**, 3865 (1996).

[36] J. P. Perdew, K. Burke, and M. Ernzerhof, Phys. Rev. Lett. **78**, 1396 (1997).

[37] F. Altorfer, B. Graneli, P. Fischer, and W. Buhrer, J. Phys.: Condens. Matter **6**, 9949 (1994).

[38] P. Haas, F. Tran, and P. Blaha, Phys. Rev. B **79**, 085104 (2009).

[39] See Supplemental Material at http://link.aps.org/supplemental/10.1103/PhysRevB.96.100301 for calculation details, comparison of measured and calculated specific heat; and Grüneisen parameters and phonon lifetimes at various pressures.

[40] P. Giannozzi, S. Baroni, N. Bonini, M. Calandra, R. Car, C. Cavazzoni, D. Ceresoli, G. L. Chiarotti, M. Cococcioni, I. Dabo, A. Dal Corso, S. de Gironcoli, S. Fabris, G. Fratesi, R. Gebauer, U. Gerstmann, C. Gougoussis, A. Kokalj, M. Lazzeri, L. Martin-Samos, N. Marzari, F. Mauri, R. Mazzarello, S. Paolini, A. Pasquarello, L. Paulatto, C. Sbraccia, S. Scandolo, G. Sclauzero, A. P. Seitsonen, A. Smogunov, P. Umari, and R. M. Wentzcovitch, J. Phys.: Condens. Matter **21**, 395502 (2009).

[41] B. Prevot, B. Hennion, and B. Dorner, J. Phys. C: Solid State Phys. **10**, 3999 (1977).

[42] G. J. Piermarini, F. A. Mauer, S. Block, A. Jayaraman, T. H. Geballe, and G. W. Hull, Solid State Commun. **32**, 275 (1979).

[43] D. L. Price, J. M. Rowe, and R. M. Nicklow, Phys. Rev. B **3**, 1268 (1971).

[44] L. Lindsay, D. A. Broido, and T. L. Reinecke, Phys. Rev. Lett. **109**, 095901 (2012).

[45] S. Mukhopadhyay, L. Lindsay, and D. S. Parker, Phys. Rev. B **93**, 224301 (2016).

[46] R. D. Shannon, Acta Crystallogr., Sect. A: Found. Adv. **32**, 751 (1976).

[47] S. Hull and D. A. Keen, J Phys.: Condens. Matter **8**, 6191 (1996).

[48] L. V. Hove, Phys. Revs **89**, 1189 (1953).

[49] A. A. Maradudin and A. E. Fein, Phys. Rev. **128**, 2589 (1962).

[50] J. M. Ziman, *Electrons and Phonons: The Theory of Transport Phenomena in Solids* (Oxford University Press, New York, 2001).

[51] E. F. Skelton, A. W. Webb, F. J. Rachford, P. C. Taylor, S. C. Yu, and I. L. Spain, Phys. Rev. B **21**, 5289 (1980).

[52] A. Ward, D. A. Broido, D. A. Stewart, and G. Deinzer, Phys. Rev. B **80**, 125203 (2009).

[53] M. G. Holland, Phys. Rev. **134**, A471 (1964).

[54] K. A. McCarthy and S. S. Ballard, J. Appl. Phys. **31**, 1410 (1960).

[55] V. A. Petrov, N. S. Tsypkina, and V. E. Seleznev, High Temp. - High Pressures **8**, 537 (1976).

[56] D. T. Morelli, V. Jovovic, and J. P. Heremans, Phys. Rev. Lett. **101**, 035901 (2008).

[57] D. A. Dalton, W. P. Hsieh, G. T. Hohensee, D. G. Cahill, and A. F. Goncharov, Sci. Rep. **3**, 2400 (2013).

[58] S. Mukhopadhyay and D. A. Stewart, Phys. Rev. Lett. **113**, 025901 (2014).